Atmos. Chem. Phys. Discuss., 7, 14461–14509, 2007
www.atmos-chem-phys-discuss.net/7/14461/2007/

Atmospheric Chemistry and Physics Discussions

The time evolution of aerosol composition over the Mexico City plateau

L. I. Kleinman[1], S. R. Springston[1], P. H. Daum[1], Y.-N. Lee[1], L. J. Nunnermacker[1], G. I. Senum[1], J. Wang[1], J. Weinstein-Lloyd[2], M. L. Alexander[3], J. Hubbe[3], J. Ortega[3], M. R. Canagaratna[4], and J. Jayne[4]

[1]Brookhaven National Laboratory, Upton, NY, USA
[2]SUNY, Old Westbury, NY, USA
[3]Pacific Northwest National Laboratory, Richland, WA, USA
[4]Aerodyne Research Inc., Billerica, MA, USA

Received: 12 September 2007 – Accepted: 20 September 2007 – Published: 11 October 2007

Correspondence to: L. I. Kleinman (kleinman@bnl.gov)

Abstract

The time evolution of aerosol concentration and chemical composition in a megacity urban plume was determined based on 8 flights of the DOE G-1 aircraft in and downwind of Mexico City during the March 2006 MILAGRO field campaign. A series of selection criteria are imposed to eliminate data points with non-urban emission influences. Biomass burning has urban and non-urban sources that are distinguished on the basis of CH_3CN and CO. In order to account for dilution in the urban plume, aerosol concentrations are normalized to CO which is taken as an inert tracer of urban emission, proportional to the emissions of aerosol precursors. Time evolution is determined with respect to photochemical age defined as $-Log_{10}$ (NO_x/NO_y). The geographic distribution of photochemical age and CO is examined, confirming the picture that Mexico City is a source region and that pollutants become more dilute and aged as they are advected towards T1 and T2, surface sites that are located at the fringe of the City and 35 km to the NE, respectively. Organic aerosol (OA) per ppm CO is found to increase 7 fold over the range of photochemical ages studied, corresponding to a change in NO_x/NO_y from nearly 100% to 10%. In the older samples the nitrate/CO ratio has leveled off suggesting that evaporation and formation of aerosol nitrate are in balance. In contrast, OA/CO increases with age in older samples, indicating that OA is still being formed. The amount of carbon equivalent to the deduced change in OA/CO with age is 56 ppbC per ppm CO. At an aerosol yield of 5% and 8% for low and high yield aromatic compounds, it is estimated from surface hydrocarbon observations that only ~9% of the OA formation can be accounted for. A comparison of OA/CO in Mexico City and the eastern U.S. gives no evidence that aerosol yields are higher in a more polluted environment.

1 Introduction

Evidence is accumulating that the mass of organic aerosol (OA) can be an order of magnitude greater than can be explained on the basis of model calculations or measurements of precursor VOCs (volatile organic compounds) (Heald et al., 2005; de Gouw et al., 2005; Volkamer et al., 2006; Cubison et al., 2006; Johnson et al., 2006; and Takegawa et al., 2006). At the same time other measurements and model calculations yield reasonable agreement (e.g. Heald et al., 2006). Interest stimulated by this problem has yielded several plausible explanations and many new findings on aerosol – gas interactions (e.g., Jang et al., 2002; Kalberer et al., 2004; Goldstein and Galbally, 2007; Robinson et al., 2007).

The Mexico City MILAGRO field campaign conducted in March, 2006 offered an excellent opportunity to investigate questions related to the production of OA in particular and the time evolution of aerosol properties in general. Eighteen million people reside in Mexico City making it one of the world's largest population centers. The region is characterized by high concentrations of gas phase and aerosol pollutants (Molina and Molina, 2002). As an example of other megacities, whose numbers are predicted to grow in the coming decades, Mexico City is both a laboratory for understanding OA production in a polluted region and an example of a globally important source category. Volkamer et al. (2006) have extrapolated results on OA production observed in Mexico City to the global aerosol budget, finding that up to 1/3 of secondary organic aerosol (SOA) could be due to anthropogenic VOCs – compared with a 6% contribution from current global models.

With these findings in mind, a focus of the MILAGRO campaign (http://www.eol.ucar.edu/projects/milagro/) and its DOE component (MAX-Mex; Megacity Aerosol Experiment in Mexico City (http://www.asp.bnl.gov/MAX-Mex.html)

was to examine the evolution of aerosols over time scales ranging from hours to days. This problem was attacked in several ways. Three surface sites were located on the Mexico City plateau in a configuration appropriate for Lagrangian sampling when

winds were from the S to SW (Doran et al., 2007). One site, T0, was located in a high emission rate section of Mexico City, while the other two, T1 and T2, were located 30 and 63 km downwind. Aircraft measurements from the G-1, augmented by several C-130 flights, were made over T0 and other parts of the city as well as on E-W transects that went over T1 and T2. This allowed for capturing plumes from Mexico City that went in a general northerly direction but happened to miss T1 and/or T2. Multi-day transport was investigated by the C-130 at locations where the Mexico City plume was predicted to be transported. A C-MET balloon was used as a Lagrangian marker. The NASA DC-8 investigated transport on still larger spatial scales, primarily over the Gulf of Mexico.

Previous studies have used a variety of sampling strategies to determine the time evolution of aerosol. Volkamer et al. (2006) relied primarily on observations in a source region, while de Gouw et al. (2005), Johnson et al. (2006), and Takegawa et al. (2006) primarily used observations from fixed receptor sites. Aircraft data from the 2004 NEAQS/ITCT campaign has been analyzed in terms of enhancements of water soluble OA and CO in individual plumes whose age is known by trajectory analysis or by ratios of reactive VOCs (Sullivan et al., 2006; Weber et al., 2007). The present study follows the approach used by Kleinman et al. (2007) in which measurements are assembled from multiple flights covering a range of photochemical ages between nearly fresh emissions and air masses that are approximately 1 day old. By using photochemical age as a metric for atmospheric processing, we take advantage of the general layout of sampling sites but are not confined to the few instances where an air mass was intercepted at multiple downwind distances.

We are mainly concerned with urban emissions over the Mexico City plateau and restrict the G-1 data set by location and by trace gas composition, the latter set of restrictions designed to minimize impacts from forest fires and industrial and utility emissions. In order to account for dilution of the urban plume with "background" air, CO is used as a conservative tracer of urban emissions and results are normalized to CO concentration. Photochemical age is marked by the oxidation of NO_x and operationally

defined as – Log_{10} (NO_x/NO_y).

This study presents results on the photochemical age dependence of SOA; organic aerosol mass peaks amu/z = 44 and 57 (M44 and M57) which are surrogates for oxygenated organic aerosol (OOA) and hydrocarbon-like organic aerosol (HOA); and other non-refractory aerosol constituents (NO_3^-, SO_4^{2-}, NH_4^+, and Cl^-) all of which are measured with an Aerodyne C-ToF-AMS. Preliminary to determining the age dependence of aerosol constituents, a set of selection criteria are described with particular attention to the use of CH_3CN and CO in identifying and removing from our data set air masses that are impacted by non-urban biomass burning. Ambient aerosol concentrations and concentrations normalized to CO are provided as a function of photochemical age. The increase with age of OA per ppm CO is compared with a calculated value based on urban measurements of aromatic hydrocarbons and literature values of aerosol yields. Comparisons are made with measurements in the eastern U.S.

2 Experimental

The G-1 was equipped with instruments to measure chemical and microphysical properties of aerosol particles as well as gases that are either aerosol precursors or tracers of emission sources. Flight time was concentrated on characterizing fresh emissions over Mexico City and determining their evolution over time durations of order 1 day or less and spatial scales of order 100 km or less.

Data used in this study are 10 s average values. Trace gas concentrations are expressed as mixing ratios by volume. Aerosol properties are reported at standard conditions of 20°C and 1 atmosphere. Local times are used in this study. Data are archived at ftp://ftp.asd.bnl.gov/pub/ASP%20Field%20Programs/2006MAXMex/. In this study flights are referred to by month (m), day (dd), and an "a" or "b" for the 1st or 2nd flight of a day, i.e. 318a for the first flight on 18 March 2006. The format for a flight identifier in the archive is yymmdda (or b), i.e., 060318a.

2.1 Flights

Measurements discussed in this paper are confined to the Mexico City plateau, west of 98° Longitude. Figure 1 shows the sampling area, surface measurement sites, and the G-1 ground track. There were 15 G-1 flights between 3 March and 27 March 2006, of which 8 had the requisite combination of measurements to examine the time evolution of aerosol properties using CO as a conservative tracer and NO_x/NO_y to determine photochemical age. Date, time and the number of transects over Legs L0 to L5 (defined in Fig. 1) are given in Table 1. Often a back and forth pattern was flown above the T1 and T2 surface sites. Altitudes above ground level (a.g.l.) were 500 to 2500 m and 200 to 2400 m for transects above the T1 and T2 surface sites, respectively. Urban crossings over T0 were mainly at an altitude of ~550 m a.g.l. The multi-stranded appearance along the L0, L1, and L2 legs is due respectively to 6, 18, and 13 overflights. As indicated in Table 1 sampling over the Mexico City plateau was distributed between mid-morning and late afternoon.

According to emission maps shown by Lei et al. (2007), T0 is located near the area of peak emission density. T1 is at the fringe of the Mexico City urban area, and T2 is 35 km outside. Figure 1 shows additional urban areas as well as the locations of the Tula power plant refinery complex, and the Popacatapetl volcano. Biomass burning on the plateau and adjacent mountains was visually observed from the G-1. Satellite observations of fires in adjacent areas are given by Yokelson et al. (2007).

2.2 Instruments

Table 2 provides a list of instruments used in this study. CO, NO_x, NO_y, and SO_2 measurements have been described by Springston et al. (2003). Acetonitrile (CH_3CN), toluene, and terpenes (and other species not used in this study) were quantified by a proton transfer mass spectrometer (PTR-MS) with a measurement cycle that was typically 15 s (Lindinger et al., 1998).

The aerosol inlet has a 50% cutoff at ~1.5 μm (Brechtel, 2003) and is not a limiting

factor for the instrumentation used in this study. Particle size between 0.1 and 3 μm was measured using a PCASP-100X (Particle Measuring Systems, Inc., Boulder, CO) with SPP-200 electronics (Droplet Measurement Technologies, Boulder, CO) mounted on an external pylon. The number distribution of particles over the size range 16 to 444 nm was determined using an SMPS consisting of a cylindrical Differential Mobility Analyzer (TSI Inc., model 3081) and a condensation particle counter (TSI Inc., model 3010). SMPS data were analyzed using the inversion procedure described by Collins et al. (2002). Aerosol size distributions are obtained at a relative humidity below 25%. For the PCASP this was achieved by using the de-icing heater (Haller et al., 2006). Air flow to the DMA passes through a Nafion dryer. In general, the atmosphere over the Mexico City plateau was very dry (average relative humidity =27%) and one would expect that particles would have little associated water even without active drying.

Non-refractory aerosol mass, composition, and size distributions were determined with an Aerodyne C-ToF AMS (Drewnick et al., 2005). A measurement cycle for acquiring a mass spectrum was typically 12 s. In this study we make use of AMS derived concentrations of organics, NO_3^-, SO_4^{2-}, NH_4^+, Cl^-, and the 44 and 57 amu/z peaks which are primarily CO_2^+ and $C_4H_9^+$, respectively. These later peaks denoted here as M44 and M57 have been used as markers for oxidized and un-oxidized hydrocarbons, respectively (Zhang et al., 2005).

The AMS collection efficiency (CE) is the fraction of particles with diameters within the acceptance range of the aerodynamic lens that actually contribute to the mass spectrometer signal. Many field studies have established that the CE of the AMS is about 0.5 (e.g. Canagaratna et al. 2006 and reference contained therein). We have evaluated CE by comparing aerosol volumes deduced from AMS measurements with that determined from the PCASP and DMA number distributions. The following preliminary steps were taken: 1) AMS concentrations were converted into volumes using the measured non-refractory speciation and densities of 1.2 and 1.77 g cm^{-3} for organic and inorganic constituents, respectively. 2) PCASP size bins which were based on an assumed refractive index of 1.55 were adjusted according to the refractive index deter-

mined from the AMS speciation using Mie scattering results from Liu and Daum (2000). As it turned out these corrections were small, typically changing the PCASP volumes by less than 10%. 3) The DMA volume for particles smaller than 100 nm was added to the PCASP volumes. These summed volumes will be referred to as PCASP volumes. The sizes of particles detected by the AMS depends on the transmission characteristics of the aerodynamic lens. Laboratory results have shown a 100% transmission for particles with a vacuum aerodynamic (va) diameter between ~60 and 600 nm (Jayne et al., 2000). At a typical aerosol density of 1.5 g cm^{-3}, the equivalent geometric diameter range of a spherical particle is 40 to 400 nm. Effects of non-spherical particles on sizing have been discussed in the literature (DeCarlo et al., 2004; Slowik et al., 2004). Particles smaller than 40 nm are not a concern in this study because their mass is negligible. Larger particles, up to 1000 nm are detected, albeit with decreased efficiency.

For each flight we have done 3 linear regression of AMS volume versus 1) PCASP volume with D_p<400 nm, 2) PCASP volume with D_p<500 nm, and, 3) DMA volume with D_p<444 nm. These sharp size cutoffs only approximate the AMS response function but in view of the decreasing amount of mass above D_p(va)=600 nm, these regressions should capture most of the information on CE. Figure 2 shows the relation between AMS volume and that from the PCASP with D_p<500 nm. Data are restricted to urban air masses as described in a following section. Similar results, with slightly shifted scales are obtained using PCASP D_p<400 nm and DMA volumes (figures not shown). According to Fig. 2, the first 7 flights show a compact relation between AMS and PCASP volume with a slope of ~0.5. Higher aerosol concentrations were observed on the 8th flight (322a) and the ratio of AMS to PCASP volume was distinctly greater than found on any of the other flights. High values of CE, above, 0.5, have been observed for acidic aerosols (Quinn et al, 2006; Kleinman et al., 2007) and CE should approach 1 for aerosol with a high proportion of NH_4NO_3 as that compound is used for calibration. Neither condition, however, applies on the 322a flight.

Consistent with results summarized in Table 3, AMS concentrations were calculated with a CE of 0.5 except for flight 322a in which CE = 0.85. Without 322a, the flight to

flight standard deviation of CE is ~0.08, possibly due to shifts in calibration or changes in aerosol-type encountered on different days.

3 Methods and supporting data

3.1 Selection criteria

Measurements made during the G-1 flights over the Mexico City plateau are affected primarily by Mexico City emissions with secondary contributions from utility and industrial sources, biomass burning, and volcanic emissions. In order to focus on the time evolution of urban emissions, data selection criteria are imposed as indicated in Table 4. These criteria have three purposes. First to restrict attention to the boundary layer over the Mexico City plateau. Second, to minimize sources of non-urban aerosols, with the exception of sulfate formed from SO_2 point sources and possibly volcanic emissions. Third, to eliminate those instances in which fresh NO_x emissions from a downwind non-urban source resets the photochemical age clock to a younger age than is appropriate for the urban mixture of pollutants. Of the aerosol that is derived from biomass burning, a fraction is from urban sources such as cooking, heating and trash incineration. To a first approximation these sources are co-located with urban CO and NO_x sources and are properly treated as part of the urban emissions whose time dependence we are interested in. The remaining biomass fraction is from fires outside the city and therefore can cause distortions in the aerosol – age relations if incorrectly attributed to urban emissions. Selection criteria should discriminate against non-urban biomass burning, hereinafter referred to as "forest fire emissions".

Once the geographic constraints and boundary layer constraints are satisfied, the primary criteria for data inclusion is that the CO/NO_y ratio be close to that observed in very polluted air masses from Mexico City, in which the pollution origin is clearly urban. As an example, Fig. 3 shows a time series from the 307a flight in which the Mexico City plume was advected to the southwest and intercepted along L4 and L5.

That the plumes in Fig. 3 represent near-by urban emissions is substantiated by the NO_x to NO_y ratio which was approximately 60%. On other flights, earlier in the day, even less processed emissions are observed with NO_x sometimes exceeding 90% of NO_y. A linear regression of the data in Fig. 3 yields $CO=98 + 20.6\ NO_y$ ($r^2=0.98$). Similar results are obtained on other flights. The criteria that:

$$15<(CO - 100)/NO_y<25 \quad (1)$$

is based on these measurements. The 15 to 25 range in Eq. (1) is greater than the spread in the urban CO to NO_y ratio but allows for uncertainties in background concentrations and for decreases in NO_y due to dry deposition of HNO_3. At concentrations approaching an ill-defined background, Eq. (1) is of limited utility so it is not used as a screening tool unless CO >170 ppb.

Industrial and utility point sources are identified as having high concentrations of SO_2 and/or a low ratio of CO to NO_y. An inspection of CO, NO_y, and SO_2 time series data (graphs not shown) indicates that the criteria in Table 4 eliminate short duration high concentration spikes which are due to near-source plume penetrations. A majority of these events are due to the Tula industrial complex. In order to obtain a representative picture of sulfate concentrations on the plateau, the SO_2 threshold is not set low enough to discriminate against all SO_2 plumes. What is important for this study is that the SO_2 plumes that are left in the data set are not otherwise different from urban pollution, in particular that the SO_2 is not associated with extra (i.e. non-urban) NO_x and CO which would affect our determination of photochemical age or dilution.

Air masses affected by forest fire emissions are identified by an elevated CH_3CN to CO ratio. Figure 4 shows the relation between CH_3CN and CO after all of the selection criteria in Table 4 have been applied except for the limits on CH_3CN and CO/NO_y. Data in Fig. 4 fall in 2 categories. There is a branch with a high CH_3CN/CO ratio due primarily to forest fires and one with a low ratio due primarily to anthropogenic sources. De Gouw et al. (2006) and Warneke et al. (2006) give examples of forest fire plumes and anthropogenic plumes which, for the most part, can be clearly differentiated on

the basis of CH_3CN/CO. Red lines in Fig. 4 indicate the range of $\Delta CH_3CN/\Delta CO$ from Alaskan and Canadian forest fires observed by de Gouw et al. (2006) near the east coast of the U.S. The area between these lines is seen to encompass much of the forest fire data in the G-1 data set. A pair of blue lines in Fig. 4 delineates a second data branch with a lower CH_3CN/CO ratio. As discussed below the CH_3CN in the low ratio branch appears to have an urban origin The upper bound of the urban branch is given by

$$CH_3CN(ppb) = 0.2 + 0.4 \times 10^{-3} CO(ppb) \quad (2)$$

An air mass is considered to have a minimal forest fire influence if it has a CH_3CN concentration below the value given in Eq. (2)

Time series data for flight 322a presented in Fig. 5 shows that CH_3CN concentrations up to 1 ppb can occur at the high CO concentrations encountered over Mexico City. On that flight a fresh urban plume (NO_y is 77% NO_x) was encountered on the L3-L4 and L0 legs between 10:00 and 11:00. CO concentrations exceed 2 ppm and the CO/NO_y ratio (see figure caption) is nearly identical to other urban transects. Hydrocarbon speciation (not shown) is also as expected for an urban source. Location, concentration, and speciation all support the contention that these plumes are composed of anthropogenic pollutants. Over most of the urban plume CO and CH_3CN concentrations are proportional, strongly suggesting a co-located source. In Fig. 5 the scales for CO and CH_3CN are related by Eq. (2) with slope and intercept qualitatively determined so as to describe the proportionality between CO and CH_3CN in these urban plumes. Having identified CO and CH_3CN as arising from common sources, and having identified the CO plumes as urban emissions, this establishes that CH_3CN concentrations up to the limit given by Eq. (2) can arise primarily from urban sources.

Urban plume points from other flights can have CH_3CN/CO slopes about a factor of two lower than that given by Eq. (2) as indicated from the bottom envelope of points in Fig. 4. This variability deserves closer attention as it may provide insights into sources of urban CH_3CN. Also shown in Fig. 4 is a least squares fit to the anthropogenic branch

which shows a CH_3CN enhancement of 0.3×10^{-3} ppb CH_3CN/ppb CO. The CH_3CN enhancement observed in Mexico City is comparable to that measured in New York City (0.25×10^{-3} ppb CH_3CN/ppb CO) by de Gouw et al. (2006).

Figure 5 includes several segments in which data is excluded from analysis because CH_3CN exceeds the value given by Eq. (2). Some of the excluded data falls within the forest fire branch defined by the de Gouw et al. (2006) data set but some of it is not clearly from anthropogenic sources or forest fires. This situation is typical of other flights. The demarcation between branches in Fig. 4 is fuzzy because there is mixing of urban and forest fire influenced air masses. Such mixing could be responsible for the relatively high concentrations of CO and CH_3CN found in less polluted "background" air masses.

In the construction of an urban-only data set, biomass burning is of most concern because models indicate that it is the dominant global source of OA (Intergovernmental Panel on Climate Change, 2001). An extrapolation of fire plume measurements made in the mountains surrounding Mexico City by Yokelson et al. (2007) indicates significant impacts on regional concentrations of CO and aerosol. In addition to the data selection criteria, forest fire data is discriminated against by determining OA/CO ratios from linear regressions which yield aerosol per CO over and above background concentrations.

3.2 Photochemical age

Exposure of pollutants to atmospheric processing is quantified using the ratio of NO_x to NO_y as a photochemical age (Olszyna et al., 1994; Kleinman et al., 2007). NO_x is emitted largely as NO which rapidly reacts with O_3 to form a steady state mixture of NO and NO_2. Subsequent oxidization reactions form HNO_3, PAN and organic nitrates. The sum total of NO_x and its oxidation products is denoted as NO_y and to a good approximation these compounds, including fine particle aerosol NO_3^-, are detected with near 100% efficiency. On the time scales of interest here, hours to 1 day, NO_y is almost conservative. Aside from rain events which were avoided, the primary NO_y removal

mechanism is by dry deposition, which is limited to a maximum loss of ~25% by the CO/NO_y constraint in Eq. (1).

We define photochemical age as $-Log_{10}$ (NO_x/NO_y), so that it has a value of 0 for fresh emissions ($NO_y = NO_x$) and a value of 1 when 90% of NO_x has been converted into oxidation products. In the daytime NO_x is primarily NO_2 and the dominant oxidation reaction is $OH + NO_2 \rightarrow HNO_3$. In that case

$$\int k[OH]dt = -2.303\,Log_{10}(NO_x/NO_y) \quad (3)$$

This relation allows us to assign a time scale to a photochemical age given an assumed OH concentration. For OH = 10^7 molec cm^{-3}, a photochemical age of 1 is reached in approximately 8 h. The average OH concentration is generally not known and there are other reactions that convert NO_x into oxidation products. Thus, Eq. (3) can only qualitatively translate a NO_x/NO_y ratio into an actual time. Assigning 10^7 OH cm^{-3} as a peak day time value, we a set a time scale of about 1 day for the transition between a photochemical age of 0 and 1.

There is an extensive literature on the use of photochemical age techniques, much of which points out ambiguities and biases in age that are inherent in atmospheric samples which contain emissions from mixtures of sources (Kleinman et al., 2003; Parrish et al., 2007, and references contained therein). While not quantitative, the NO_x/NO_y clock (in common with VOC clocks) should be monotonic if significant downwind emissions sources are avoided as we attempt to do by screening out non-urban NO_x plumes. It is therefore a useful metric for ordering air masses according to atmospheric exposure.

Because Mexico City is the major source of NO_x on the plateau it is expected that photochemical age will be low over the city and increase towards the T1 and T2 downwind sites. That is shown in Fig. 6. Although flights were preferentially scheduled for days when transport would be from the city to the L2 leg (Doran et al., 2007), the general increase in age with distance away from the city is not necessarily due to direct

transport. As long as there are flows in the basin mixing material outward from the source region, the behavior shown in Fig. 6 is expected.

3.3 Dilution

As Mexico City emissions are transported away from their source region they become dilute due to a mixing-in of cleaner air from elsewhere. We account for dilution in the determination of age-related changes to aerosol properties by normalizing results to CO, which, on the time scales of interest is a conservative tracer. Because of the selection criteria in Table 4, CO concentrations above background are mainly from urban emissions. It is assumed that emission sources for aerosols and their precursors are co-located with CO sources either because these compounds are emitted from a common source type (i.e. diesel vehicles) or because they are emitted in proportion to a common factor such as population density. On this basis,

$$E_{POA} = \alpha E_{CO}$$
$$[POA - OA_B] = \alpha[CO - CO_B] \quad (4)$$

where E's are emission rates, POA is primary organic aerosol, square brackets indicate concentration, subscript B indicates a background value, and α is a proportionality constant. Before any SOA is formed, OA is identical to POA. SOA production is evidenced from the ratio $[OA–OA_B]/[CO–CO_B]$ increasing above α to, say α'. Note that α' can be evaluated without knowing background concentrations by

$$\alpha' = d[OA]_i/d[CO]_i \quad (5)$$

where subscript "i" identifies a data sub set with a particular photochemical age. Similar consideration apply to other aerosol components.

Dilution of pollutants on the Mexico City plateau is illustrated in Fig. 7. As expected highest concentrations of CO are located over the city and concentrations are progressively lower over L1 and L2, which as shown in Fig. 6 tend to be where older air masses are located. On each leg there is a spectrum of CO concentrations and ages which

reflects flight to flight differences in plume location and ventilation. By almost any measure a non-city CO concentration of 200 to 300+ ppb such as observed on L2 is very high. In this case, peak concentrations over the city are sufficiently high that a 300 ppb downwind concentration can be consistent with the good ventilation that is predicted by particle dispersion calculations (Fast and Zhong, 1998; de Foy et al., 2006)

A decrease in CO concentration as a function of photochemical age is shown in Fig. 8a. Peak CO concentrations reach 2.5 ppm. For ages greater than 0.5, CO concentration vary between 100 and more than 300 ppb, with an average of ∼180 ppb which does not decrease significantly with age. (There were a few CO measurements below 100 ppb which are most likely not boundary layer air and are removed from our data set according to the selection criteria in Table 4.) An analogous dilution graph for organic aerosol is shown in Fig. 8b. The age dependence of organic aerosol is clearly different than CO indicating that the ratio OA/CO increases with age. This finding is put on a firmer footing in the next section.

4 Age dependence of normalized aerosol concentration

At this point we have limited the G-1 data set to urban emissions and have described the use of CO as a conservative tracer and the oxidation of NO_x as a way of determining photochemical age. In a previous study (Kleinman et al., 2007) we constructed ratios such as OA/CO by subtracting background values for OA and CO. In Mexico City, aged air masses can have high and variable concentrations of trace gas and aerosols, as illustrated in Fig. 8. It is problematic to define background conditions.

Instead we have divided the data set into 10 subsets, each spanning 0.1 units of age. Subsets have over 100 data points except for the youngest (39) and oldest (50). For each subset a linear least squares regressions was performed with total AMS aerosol concentration or organic aerosol concentration as the dependent variables (Y) and CO as the independent variable (X). Regression slopes are determined from the reduced major axis approach which, according to Isobe et al. (1990), is appropriate when "the

objects under study have an intrinsic scatter that is much larger than the uncertainties due to the measurement process". In this approach the slope is the geometric mean of the ordinary least squares regression slope of Y vs. X and one over the slope of X vs. Y. As it is assumed that CO is a conservative tracer of the urban plume which is also the source of aerosols and aerosol precursors, these slopes represent urban aerosol impacts normalized to account for dilution.

The age dependence of aerosol components after accounting for dilution is determined from

$$d[X]/d[CO]_i = d[Aerosol]/d[CO]_i \times Average([X]/[Aerosol])_i \quad (6)$$

where X can be organics, nitrate, sulfate, ammonium, or chloride and i is an index for photochemical age. One gets slightly different results with this approach compared to a regression of individual species versus CO (as is done for organics). Equation (6), however, has the advantage that the 5 components are guaranteed to add up to the total aerosol concentration. The age dependence of ambient aerosol (without accounting for dilution) is simply given by $[X]_i$.

In order to summarize the time evolution of aerosol we define an age growth factor, G, which is the fractional change in concentration between the youngest and oldest age bins. This factor is defined with respect to the value of a linear least squares fit, i.e. if

$$d[X]/d[CO]=a + b \times Age$$

then G is given by

$$G=(a + bAge_{10})/(a + bAge_1) \quad (7)$$

where Age_1 and Age_{10} are average ages in the first and last age bins, 0.083 and 0.94, respectively. Changes in aerosol between zero age and 0.083 are not included in G because there are too few measurements to support an extrapolation of the least squares fit.

Figure 9 shows the time evolution of total non-refractory aerosol and organic aerosol, normalized to CO, based on the regression analysis described above. It was not possible to determine a priori the errors in aerosol concentration and CO since the variability in Aerosol/CO has a not-easily-quantified component from atmospheric heterogeneity. Instead error bounds are calculated from χ^2 according to the method in Press et al. (1986). Error bars are largest for the youngest and two oldest data subsets, which have a smaller number of samples and/or a poor correlation compared to other data subsets.

A linear least squares fit has been added to Fig. 9 as a description of the increase in these quantities as functions of photochemical age. According to Eq. (7), there is a factor of 5.0 and 6.9 increase in dilution-corrected total aerosol and organic aerosol due to photochemical aging.

Normalized aerosol composition calculated as a function of photochemical age according to Eq. (6) is shown in Fig. 10a. There is a more or less uniform increase in total aerosol concentration with age, except for a dip in the 2 age bins between 0.6 and 0.8, which is discussed below. Compared to young air masses, aged air masses tend to have a higher proportion of organics and sulfate and a lower proportion of nitrates. Ammonium concentrations vary with nitrate and sulfate so as to yield a nearly age-independent neutralization of 88–99%. Aerosol age growth factors based on the data in Figs. 9a, 9b, and 10a are given in Table 5.

Figure 11 presents average ambient aerosol concentrations for 10 age bins. Although aerosol/CO increases several-fold with age, dilution causes actual aerosol concentrations to be lowest in older air masses. Ambient levels of the 5 aerosol constituents can be reconstructed by multiplying the "per CO" concentrations in Fig. 10a by the average CO concentrations in Fig. 10b, taking care to subtract background CO. Background CO is actually a difficult quantity to determine directly from the data which is why the "per CO" concentrations were derived from a regression analysis. Figure 11 includes re-constructed total aerosol concentrations determined from

$$[\text{Aerosol}]_{\text{Reconstructed}} = (\text{Aerosol/CO}) \times [\text{CO} - \text{CO}_{\text{B}}] \quad (8)$$

where Aerosol/CO is the data in Fig. 10a, CO concentrations are from Fig. 10b, and background CO is set at 100 ppb. There is good agreement between reconstructed and measured aerosol. This agreement implies that in the clean conditions represented by a 100 ppb CO concentration, background aerosol concentrations are near zero. An inspection of the CO data, however, shows that the low concentration points cluster near 130 ppb. If we take this value as background and evaluate Eq. (8) we get a second reconstructed aerosol concentration that is on average 3 μg m^{-3} lower than previously obtained. Except for the 1st age bin, the reconstructed aerosol is 2 to 4.5 μg m^{-3} lower than the observed ambient, which we can assign as background aerosol. As seen by these 2 reconstructions, background aerosol is sensitive to assumptions on background CO. It is encouraging that over a reasonable range of CO concentrations, reasonable predictions for background aerosol result.

Age trends in M44/Org and M57/Org are shown in Fig. 12. With atmospheric aging the proportion of M44 is seen to increase and the proportion of M57 to decrease. This is consistent with two identifications made by Zhang et al. (2005): first that M44 and M57 are approximate surrogates for OOA and HOA, and second that that OOA and HOA have the properties of SOA and POA. The increase in M44 and the decrease in M57 then follows when the addition of organic mass with age is accomplished by adding SOA to pre-existing aerosol.

5 Discussion

5.1 Non-uniform sources

Compared to the linear fits, the data points in Figs. 9 and 10 show some bumps and dips, the largest being low values in the age bins 0.6–0.7 and 0.7–0.8. This feature is due to a collection of points from flight 320b, located just to the east of the L2 leg. At this location, 18 km of a high CO plume was sampled, with almost identical results at 3 altitudes. These data points are visible in Fig. 8a as a group with CO~400 ppb that are

detached from the more numerous lower concentration points at the same photochemical age. According to the selection criteria in Table 4 and other measurements, there is nothing else unusual about this plume. Yet, something is different and the high CO concentrations yield low values for the dilution corrected quantities in Figs. 9 and 10. Effects of removing this plume are shown in Fig. 9. The premise of a uniform mixture of emissions is a good approximation but there are exceptions.

5.2 Aerosol composition

Most of the non-refractory mass measured by the AMS is of secondary origin, as shown in the previous section for organics. For sulfate, nitrate, and ammonium ions, gas to particle conversion, augmented by aqueous phase chemistry in the case of SO_4^{2-}, are known to be the major pathway for adding these materials to the aerosol phase. The addition of secondary material to the aerosol phase will cause concentrations, normalized to CO, to increase. Sulfate is non-volatile, so additions to the aerosol phase are not reversible. NH_4^+ and NO_3^-, are volatile. If aerosols are advected into regions with low partial pressures of NH_3 and HNO_3, these substances can evaporate. Although the age dependence of dilution-adjusted aerosol concentrations are affected by many processes besides volatility, the behavior of nitrate suggests that partitioning between gas and aerosol phases is important (Lee et al., 2006). Aerosol nitrate concentrations (Fig. 10a) are almost constant above a photochemical age of 0.4 causing the age growth factor to be the lowest in Table 5. On average, a point has been reached where aerosol nitrate growth balances loss. Presumably, individual samples gain or loose of nitrate depending on conditions. Organic aerosol concentration (Fig. 10a), in contrast, continues to increase over the entire age range. Although it is possible that the average includes some samples in which OA is evaporating, the overall trend suggests that this is not a dominant process.

5.3 Carbon mass balance

In this section we estimate the gas phase hydrocarbon precursor concentrations required to account for the 6.9 fold increase in organic aerosol that occurs during aging. The increase in aerosol concentration, normalized to CO, is given by

$$\Delta(\mathrm{OA/CO}) = (\mathrm{OA/CO})_{\mathrm{LSQ(10)}} - (\mathrm{OA/CO})_{\mathrm{LSQ(1)}} \quad (9)$$

where the value of OA/CO is evaluated at the 2 endpoints of the linear least squares fit shown in Fig. 9b. Equation (9) yields Δ(OA/CO) = 62 μg m^{-3}/ppm CO. It is assumed that the organic mass added during aging is OOA with a carbon content, OC, given by OOA/OC = 2.2 μg/μg C (Zhang et al., 2005). The carbon added to the aerosol phase during aging is then Δ(OC/CO) = 28 μg C m^{-3}/ppm CO, equivalent to 56 ppbC per ppm CO.

The next step is to determine the amount of organic aerosol that would be produced from gas phase precursors. Our calculations are based on Mexico City surface urban aromatic hydrocarbon (HC) measurements reported by Velasco et al. (2007) in their Table 4. Velasco et al. 2007 do not report CO measurements, so conversion into ppb HC/ppm CO is accomplished by using toluene as a transfer standard. PTR-MS observations coincident with the aerosol data set used in this study yield the following relation:

$$[\mathrm{toluene(ppb)}] = -0.48 + 4.2\,[\mathrm{CO(ppm)}],\ r^2 = 0.85 \quad (10)$$

which is equivalent to 29 ppbC per ppm CO. Thus, the inferred increase in OA is stoichiometrically equivalent to 193% of ambient toluene. Hydrocarbon/CO ratios are obtained by combining Eq. (10) with the surface HC observations, yielding

$$\mathrm{HC\,(ppb)/CO\,(ppm)} = (\mathrm{HC/toluene})_{\mathrm{Surface}} \times (4.2\,\mathrm{ppb\,toluene/ppm\,CO})_{\mathrm{G-1}} \quad (11)$$

Smog chamber data for low and high yield aromatic OA precursors, presented by Odum et al. (Fig. 1, 1997) give an aerosol yield of 5% and 8%, respectively, at an OA concentration of 100 μg m^{-3}. According to the gas/aerosol absorptive partitioning model

(Pankow, 1994) and the data of Odum et al. 1997, aerosol yields increase as the organic aerosol phase available for partitioning is made larger. Yields used here are likely to be overestimates for the G-1 data set as ambient organic aerosol concentrations were considerably lower than 100 $\mu g\,m^{-3}$ (see Fig. 11). Organic aerosol production is calculated from

$$\Delta(\text{OA ppbC/ppm CO})_{\text{Predicted}} = \sum(\text{ppbC HC}_i/\text{ppm CO}) \times Y_i \quad (12)$$

where Y_i is the aerosol yield of the ith compound and the sum includes 13 aromatic compounds measured by Velasco et al. (2007). The predicted OA formation is 4.8 ppbC per ppm CO, 2.4 ppbC of which is from toluene. Equation (12) accounts for only 9% of the observed 56 ppbC per ppm CO added to the aerosol phase in aging.

The obvious question is: Where does the additional 51 ppbC/ppm CO accounting for 91% of the organic aerosol mass added during aging come from? Other anthropogenic precursors with significant organic aerosol yields include longer chain alkanes and alkenes (Seinfeld and Pandis, 1998). In a simulation of aerosol formation in Mexico City these compounds added only another 25% to the aerosol yields from aromatics (Volkamer et al., 2006). Biogenic VOCs have high aerosol yields (Griffin et al., 1999) but the G-1 PTR-MS measurements of terpenes were typically less than 0.2 ppb. Another pathway for organic aerosol production is partitioning of hydrophilic VOCs into the aerosol aqueous phase (Aumont et al., 2000). However, in most models (e.g. Griffin et al., 2002) this mechanism is of lesser importance than the addition of hydrophobic compounds typified by oxidation products of aromatics. Enhanced yields from acid catalyzed reactions seem unlikely because Mexico City aerosols are nearly neutralized. Furthermore, recent studies have not found evidence that aerosol yields increase with acidity under the range of conditions encountered in the ambient atmosphere (Peltier et al., 2007; Zhang et al., 2007). It is possible that extra sources of organic aerosol are to be found among high molecular weight, low and intermediate volatility VOCs (Goldstein and Galbally, 2007; Robinson et al., 2007). Such compounds could include oxidation products of VOCs that are evaporated from POA during the rapid dilution that

occurs shortly after emission (Robinson et al., 2007). Aerosol phase polymerization reactions that yield non-volatile products are another possibility (Kalberer et al., 2004). Such a mechanism would be consistent with the apparent lack of an evaporative loss of OA (in fact a continued growth) as an air mass ages and gas phase concentrations decrease.

Organic aerosol mass in excess of model predictions has been observed in several locations using different methodologies. Of most relevance to the present study are the observations of Volkamer et al. (2006) at the CENICA urban site in Mexico City during April, 2003. Model calculations that were based on measured oxidants and VOCs accounted for less than 1/8th of the OOA increase at CENICA between sunrise and mid-afternoon. De Gouw et al. (2005) reach a similar conclusion based on observations up to 2 days downwind of the northeastern U.S. coast, namely that measured anthropogenic aerosol precursors could only account for 7% of the observed SOA, with little likelihood that biogenic compounds could make up much of the difference.

5.4 Comparison with the Eastern U.S.

Mexico City has a more concentrated set of emission sources than found in most, if not all, areas of the U.S. resulting in very high concentrations of gas phase pollutants (Figs. 3 and 5; Molina and Molina, 2002). Our emphasis in this study, however, has been on intensive properties, in particular on OA production per unit CO. It is of interest to determine whether this intensive property depends on absolute concentration. If it does, then the growth of megacities would lead to a different set of impacts compared to the situation where the same number of people and the same amount of industrial activity are spread out over several smaller population centers. An expectation that Δ(OA/CO) might be greater in regions with high emissions can be justified on the basis of the absorptive/ partitioning model, in which aerosol yields increase when there is a large amount of organics in the aerosol phase into which low volatility VOCs can partition.

In Table 6 we compare Δ(OA/CO), calculated from Eq. (9) with the correspond-

ing quantity calculated from the 2002 NEAQS (Kleinman et al., 2007) and 2004 NEAQS/ITCT (Sullivan et al., 2007; Weber et al., 2007) field campaigns. The 2002 and 2004 NEAQS studies used data from the northeastern U.S. and in 2004 also from northern GA. As a qualitative indicator of pollution levels, CO concentrations in Mexico City reached 2.5 ppm, while those measured in the U.S., which included plumes from NYC and Atlanta, had CO below 325 ppb. On average, CO concentrations in Mexico City were twice that observed in the 2002 NEAQS campaign.

The amount of OA produced during aging in Mexico City is 62 $\mu g\,m^{-3}$ per ppm CO, as compared to 66 and 63 $\mu g\,m^{-3}$ per ppm CO for the 2002 and 2004 NEAQS studies. This comparison offers no evidence that OA production per CO in Mexico City is any greater than in the eastern U.S.

There are a few caveats to the comparison: 1) In all 3 studies OA is normalized to CO as a tracer of urban emissions. The utility of CO rests on the assumption that CO is emitted in proportion to compounds that are responsible for OA production. While this assumption may hold within a region, emission sources in Mexico City and the eastern U.S. do differ. Further work is needed to determine how per-CO numbers translate from one region to another. 2) Related to item 1 are differences in biogenic emissions which are sources of SOA that are not expected to be correlated with CO. 3) Comparisons should be performed over the same time interval. The one day aging time for Mexico City estimated from NO_x/NO_y is less accurate than back trajectory ages determined for most of the 2004 NEAQS data. If the older Mexico City samples have undergone less aging than the older NEAQS samples this would make the Mexico City Δ(OA/CO) appear to be low. 4) The 2004 results should be considered a lower bound as organic aerosol measurements are of the water soluble component – operationally defined as the aerosols that grow into a collectible size when exposed to supersaturated conditions within the PILS. 5) There were few near-source measurements in the 2002 NEAQS campaign and the inferred value of OA/CO at low age is relatively uncertain. 6) Even though very high gas phase pollutant concentrations are encountered in Mexico City, a comparison of Fig. 8b and 11 with Fig. 9 of Kleinman et al. (2007)

indicates comparable OA concentrations in both regions. We defer a comparison of absolute concentrations except to note that OA in the NEAQS region was uncharacteristically high compared with long term monitoring data from the IMPROVE network (Malm et al., 2004).

Our results leave open the possibility that more "efficient" OA production would have been observed in Mexico City if there were stagnation events such that pollutants aged under more concentrated conditions.

6 Conclusions

Changes in aerosol concentration and speciation have been determined as a function of photochemical age based on 8 flights of the DOE G-1 aircraft in and downwind of Mexico City. Over the City we find young concentrated plumes, with CO concentrations up to 2.5 ppm and NO_x/NO_y ratios that can exceed 90%. Successively lower CO concentrations and older air masses are found over the T1 and T2 surface sites. The measurements considered here are confined to the Mexico City plateau and yield almost an order of magnitude spread in photochemical age defined as $-Log_{10}(NO_x/NO_y)$. A qualitative estimate of age since emission is less than 1 h to about 1 day.

Our interest is in the evolution of urban plumes and towards that end a set of selection criteria were imposed to eliminate air masses significantly impacted by non-urban biomass burning and utility and industrial sources. Forest fire plumes are known to have elevated CH_3CN/CO ratios (de Gouw et al., 2006; Warneke et al., 2006). An inspection of data taken in well defined urban plumes supports a designation that pollutants were primarily urban if $CH_3CN(ppb) < 0.2 + 0.4 \times 10^{-3} CO\,(ppb)$. Because CO concentrations could reach more than 2 ppm, the urban source of CH_3CN could contribute over 1 ppb CH_3CN, presumably from embedded burning such as cooking, heating, and waste incineration.

As an air massed aged from the youngest to oldest category the fraction of aerosol that was organic increased from ∼50 to 60%, nitrate decreased from ∼25 to 10%,

and sulfate increased from ∼7 to 17%. At all ages, ammonium concentrations were sufficient to neutralize ∼90 to 100% of the aerosol acidity from sulfate and nitrate. With increasing age M44/OA increases and M57/OA decreases, consistent with the added OA mass being OOA.

The urban data set was split into 10 subsets and for each the amount of aerosol per ppm CO was determined as the slope of a linear regression. This procedure has the advantage that one does not have to specify background concentrations which are difficult to estimate. Between the youngest and oldest data subset, total non-refractory aerosol measured by an AMS increased by a factor of 5, while organics showed a 7 fold increase. OA/CO shows a steady increase with no sign that OA is evaporating in older air masses, in which lower gas phase VOC concentrations might be expected to cause re-partitioning of semi-volatile organic compounds back into the gas phase. Nitrate/CO, in contrast, has reached a plateau suggesting that condensation and evaporation of NH_3 and HNO_3 are in balance. Upon multiplying the per CO aerosol concentrations by an average CO above background, one recovers reasonable conditions, i.e. background aerosol = 2–4.5 $\mu g\,m^{-3}$ at CO = 130 ppb.

The change in OA/CO between the youngest and oldest age bins is 62 $\mu g\,m^{-3}$ per ppm CO. At an OC/OA ratio characteristic of OOA (Zhang et al., 2005) this is equivalent to 56 ppbC per ppm CO. OA production calculated from surface HC measurements (Velasco et al., 2007) and smog chamber data (Odum et al., 1997) can only explain 9% of the inferred increase in OA during aging, a fraction similar to what others have found (de Gouw et al., 2005; Volkamer et al., 2006). Continued OA formation over 1 day is consistent with mechanisms in which low volatility VOC are continuously produced and/or aerosol-phase polymerization reactions yield low volatility products such that OA does not re-partition to the gas phase in cleaner air.

OA production was compared with observations made in the eastern U.S. during the 2002 NEAQS (Kleinman et al., 2007) and 2004 NEAQS/ITCT (Sullivan et al., 2006; Weber et al., 2007) field campaigns. In approximately 1 days aging, similar amounts of OA were produced per unit CO. We find no evidence for a megacity effect, whereby

conversion of OA precursors to OA proceeds to a greater extent in a region with very high emission rates.

Acknowledgements. We thank chief pilot B. Hannigan and the flight crew from PNNL for a job well done. We gratefully acknowledge the Atmospheric Science Program within the Office of Biological and Environmental Research of DOE for supporting field and analysis activities and for providing the G-1 aircraft. Use of a PTR-MS provided by EMSL is appreciated. The MILAGRO campaign owes its success to many people. We would like to single out L. Molina (MIT and MCE2), S. Madronich (NCAR) and J. Gaffney (Univ. Arkansas) for organizational efforts and scientific guidance, and J. Fast (PNNL) and colleagues for weather and pollution forecasts. We thank D. Sueper (Aerodyne and Univ. CO) for her assistance in reducing the AMS data. This research was performed under sponsorship of the U.S. DOE under contracts DE-AC02-98CH10886.

References

Aumont, B., Madronich, S., Bey, I., and Tyndall, G. S.: Contribution of secondary VOC to the composition of aqueous atmospheric particles: A modeling approach, J. Atmos. Chem. Phys., 35, 59–75, 2000, http://www.atmos-chem-phys.net/35/59/2000/.

Brechtel, F. J.: Description and Assessment of a New Aerosol Inlet for the DOE G-1 Research Aircraft. Final Technical Report of work performed by BMI under contract #0000058843 to Brookhaven National Laboratory, Aug., 2003.

Canagaratna, M. R., Jayne, J. T., Jimenez, J. L., et al.: Chemical and microphysical characterization of ambient aerosol with the Aerodyne Aerosol Mass Spectrometer, Mass Spectrom. Rev., 26, 185–222, doi:10.1002/mas.20115, 2007.

Collins, D. R., Flagan, R. C., and Seinfeld, J. H.: Improved inversion of scanning DMA data, Aerosol Sci. Technol., 36(1), 1–9, 2002.

Cubison, M. J., Alfarra, M. R., Allan, J., Bower, K. N., Coe, H., McFiggans, G. B., Whitehead, J. D., Willimams, P. I., Zhang, Q., Jimenez, J. L., Hopkins, J., and Lee, J.: The characterisation of pollution aerosol in a changing photochemical environment, Atmos. Chem. Phys., 6, 5573–5588, 2006, http://www.atmos-chem-phys.net/6/5573/2006/.

DeCarlo, P., Slowik, J. G., Worsnop, D. R., Davidovits, P., and Jimenez, J. L.: Particle morphology and density characterization by combined mobility and aerodynamic

diameter measurements. Part 1: Theory, Aerosol Sci. Technol., 38, 1185–1205, doi:10.1080/027868290903907, 2004.
de Foy, B., Varela, J. R., Molina, L. T., and Molina, M. J.: Rapid ventilation of the Mexico City basin and regional fate of the urban plume, Atmos. Chem. Phys., 6, 2321–2335, 2006, http://www.atmos-chem-phys.net/6/2321/2006/.
de Gouw, J. A., Middlebrook, A. M., Warneke, C., Goldan, P. D., Kuster, W. C., Roberts, J. M., Fehsenfeld, F. C., Worsnop, D. R., Canagaratna, M. R., Pszenny, A. A. P., Keene, W. C., Marchewka, M., Bertman, S. B., and Bates, T. S.: Budget of organic carbon in a polluted atmosphere: Results from the New England Air Quality Study in 2002, J. Geophys. Res., 110, D16305, doi:10.1029/2004JD005623, 2005.
de Gouw, J. A., Warneke, C., Stohl, A., et al.: Volatile organic compounds composition of merged and aged forest fire plumes from Alaska and western Canada, J. Geophys. Res., 111 D10303, doi:10.1029/2005JD006175, 2006.
Doran, J. C., Barnard, J. C., Arnott, W. P., et al.: The T1-T2 study: evolution of aerosol properties downwind of Mexico City, Atmos. Chem. Phys., 7, 1585–1598, 2007
Drewnick, F., Hings, S. S., DeCarlo, P. F., Jayne, J. T., Gonin, M., Fuhrer, K., Weimer, S., Jimenex, J. L., Demerjian, K. L., Borrmann, S., and Worsnop, D. R.: A new Time-of-Flight Aerosol Mass Spectrometer (ToF-AMS) – Instrument description and first field deployment, Aerosol. Sci. Technol., 39, 637–658, 2005.
Fast, J. D. and Zhong, S.: Meteorological factors associated with inhomogeneous ozone concentrations within the Mexico City basin, J. Geophys. Res., 103, D15, 18 927–18 946, 1998.
Goldstein, A. H. and Galbally, I. E.: Known and unexplored organic constituents in the Earth's atmosphere, Environ. Sci. Technol., 41(5), 1514–1521, 2007.
Griffin, R. J., Cocker III, D. R., Flagan, R. C., and Seinfeld, J. H.: Organic aerosol formation from the oxidation of biogenic hydrocarbons, J. Geophys. Res., 104(D3), 3555–3567, 1999.
Griffin, R. J., Daddub, D., Kleeman, M. J., Fraser, M. P., Cass, G. R., and Seinfeld, J. H.: Secondary organic aerosol 3. Urban/regional scale model of size-and composition-resolved aerosols, J. Geophys. Res., 107(D17), doi:10.1029/2001JD000544, 2002.
Haller, A. G., Strawa, A. W., Schmid, B., Andrews, E., Ogren, J., Sheridan, P., Ferrare, R., Covert, D., Elleman, R., Jonsson, H., Bokarius, K., and Luu, A.: Atmospheric Radiation Measurements Aerosol Intensive Operating Period: Comparison of aerosol scattering during coordinated flights, J. Geophys. Res., 111, D05S09, doi:10.1029/2005JD006250, 2006.
Heald, C. L., Jacob, D. J., Park, R. J., Russell, L. M., Huebert, B. J., Seinfeld, J. H., Liao, H., and

Weber, R. J.: A large organic aerosol source in the free troposphere missing from current models, Geophys. Res. Lett., 32, L18809, doi:10.1029/2005GL023831, 2005.
Heald, C. L., Jacob, D. J., Turquety, S., et al.: Concentrations and sources of organic carbon compounds in the free troposphere over North America, J. Geophys. Res., 111, D23S47, doi:10.1029/2006JD007705, 2006.
Intergovernmental Panel on Climate Change: Climate Change 2001 – The Scientific Basis, edited by: J. T. Houghton et al., Cambridge Univ. Press, 2001.
Isobe, T., Feigelson, E. D., Akritas, M. G., and Babu, G. J.: Linear regression in astronomy, I., The Astrophysical Journal, 364, 104–113, 1990.
Jang, M., Czoschke, N. M., Lee, S., and Kamens, R. M.: Heterogeneous atmospheric aerosol production by acid-catalyzed particle-phase reactions, Science, 298, 814–817, 2002.
Jayne, J. T., Leard, D. C., Zhang, X., Davidovits, P., Smith, K. A., Kolb, C. E., and Worsnop, D. R.: Development of an aerosol mass spectrometer for size and composition analysis of submicron particles, Aerosol Sci. Technol., 33, 49–70, 2000.
Johnson, D., Utembe, S. R., Jenkin, M. E., Derwent, R. G., Hayman, G. D., Alfarra, M. R., Coe, H., and McFiggans, G.: Simulating regional scale secondary organic aerosol formation during the TORCH 2003 campaign in the southern UK, Atmos. Chem. Phys., 6, 403–418, 2006, http://www.atmos-chem-phys.net/6/403/2006/.
Kalberer, M., Paulsen, D., Sax, M., Steinbacher, M., Dommen, J., Prevot, A. S. H., Fisseha, R., Weingartner, E., Frankevich, V., Zenobi, R., and Baltensperger, U.: Identification of polymers as major constituents of atmospheric organic aerosols, Science, 303, 1659–1662, 2004.
Kleinman, L. I., Daum, P. H., Lee, Y.-N., Nunnermacker, L. J., Springston, S. R., Weinstein-Lloyd, J., Hyde, P., Doskey, P., Rudolph, J., Fast, J., and Berkowitz, C.: Photochemical age determinations in the Phoenix metropolitan area, J. Geophys. Res., 108(D3), 4096, doi:10.1029/2002JD002621, 2003.
Kleinman, L. I., Daum, P. H., Lee, Y.-N., Senum, G. I., Springston, S. R., Wang, J., Berkowitz, C., Hubbe, J., Zaveri, R. A., Brechtel, F. J., Jayne, J., Onasch, T. B., and Worsnop, D.: Aircraft observations of aerosol composition and ageing in New England and Mid-Atlantic States during the summer 2002 New England Air Quality Study field campaign, J. Geophys. Res., 112, D09310, doi:10.1029/2006JD007786, 2007.
Lee, Y.-N., Jayne, J., Alexander, L., Canagaratna, M., Springston, S. R., Senum, G. I., Hubbe, J., Daum, P. H., and Kleinman, L.: Aerosol composition determined on board the DOE G-1 aircraft during MAX-Mex in March 2006, First MILAGRO Science Meeting, Boulder, CO, 23

Oct., 2006.
Lei, W., de Foy, B., Zavala, M., Volkamer, R., and Molina, L.T.: Characterizing ozone production in the Mexico City Metropolitan Area: a case study using a chemical transport model, Atmos. Phys., 7, 1347–1366, 2007.
Lindinger, W., Hansel, A., and Jordan, A.: On-line monitoring of volatile organic compounds at pptv levels by means of Proton-Transfer Mass Spectrometry (PTR-MS) medical applications, food control, and environmental research, Int. J. Mass Spectrum. Ion Process 173, 191–241, 1998.
Liu, Y. and Daum, P. H.: The effect of refractive index on size distributions and light scattering coefficients derived from optical particle counters, J. Aerosol Sci., 8, 945–957, 2000.
Malm, W. C., Schichtel, B. A., Pitchford, M. L., Ashbaugh, L. L., and Eldred, R. A.: Spatial and monthly trends in speciated fine particle concentration in the United States, J. Geophys. Res., 109, D03306, doi:10.1029/2003JD003739, 2004.
Molina, L. T. and Molina, M. J.: Air Quality in the Mexico Megacity: An Integrated Assessment, Kluwer Academic Publishers, 2002.
Odum, J. R., Jungkamp, P. W., Griffin, R. J., Forstner, H. J. L., Flagan, R. C., and Seinfeld, J. H.: Aromatics, reformulated gasoline, and atmospheric organic aerosol formation, Environ. Sci. Technol., 31, 1890–1897, 1997.
Olszyna, K. J., Bailey, E. M., Simonaitis, R., and Meagher, J. F.: O_3 and NO_y relationships at a rural site, J. Geophys. Res., 99, 14 557–14 563, 1994.
Pankow, J. F.: An absorption model of the gas/aerosol partitioning involved in the formation of secondary organic aerosol, Atmos. Environ, 28, 189–193, 1994.
Parrish, D. D., Stohl, A., Forster, C., Atlas, E. L., Blake, D. R., Goldan, P. D., Kuster, W. C., and de Gouw, J. A.: Effects of mixing on evolution of hydrocarbon ratios in the troposphere, J. Geophys. Res., 112, D10S34, doi:10.1029/2006JD007584, 2007.
Peltier, R. E., Sullivan, A. P., Weber, R. J., Wollny, A. G., Holloway, J. S., Brock, C. A., de Gouw, J. A., and Atlas, E. L.: No evidence for acid-catalyzed secondary organic aerosol formation in power plant plumes over metropolitan Atlanta, Georgia, Geophys. Res. Lett., 34, L06801, doi:10.1029/2006GL028780, 2007.
Press, W. H., Flannery, B. P., Teukolsky, S. A., and Vetterling, W. T.: Numerical Recipes, The Art of Scientific Computing, Cambridge University Press, p. 507, 1986.
Quinn, P. K., Bates, T. S., Coffman, D., et al.: Impacts of sources and aging on submicrometer aerosol properties in the marine boundary layer across the Gulf of Maine, J. Geophys. Res.,

111, D23S36, doi:10.1029/2006JD007582, 2006.
Robinson, A. L., Donahue, N. M., Shrivastava, M. K., Weitkamp, E. A., Sage, A. M., Greishop, A. P., Lane, T. E., Pierce, J. R., and Pandis, S. N.: Rethinking organic aerosol: Semivolatile emissions and photochemical aging, Science, 315, 1259–1262, 2007.
Seinfeld, J. H. and Pandis, S. N.: Atmospheric Chemistry and Physics, From Air Pollution to Climate Change, ISBN 0-471-17816-0, John Wiley & Sons, 1998.
Slowik, J. G., Stainken, K., Davidovits, P., Williams, L. R., Jayne, J. T., Kolb, C. E., Worsnop, D. R., Rudich, Y., DeCarlo, P., and Jimenex, J. L.: Particle morphology and density characterization by combined mobility and aerodynamic diameter measurements. Part 2: Application to combustion generated soot particles as a function of fuel equivalence ratio, Aerosol Sci. Technol., 38, 1206–1222, doi:10.1080/027868290903916, 2004.
Springston, S. R., Kleinman, L. I., Brechtel, F., Lee, Y.-N., Nunnermacker, L. J., and Wang, J.: Chemical evolution of an isolated power plant plume during the TexAQS 2000 study, Atmos. Environ., 39, 3431–3443, 2005.
Sullivan, A. P., Peltier, R. E., Brock, C. A., de Gouw, J. A., Holloway, J. S., Warneke, C., Wollny, A. G., and Weber, R. J.: Airborne measurements of carbonaceous aerosol soluble in water over northeastern United States: Method development and an investigation into water-soluble organic carbon sources, J. Geophys. Res., 111, D23S46, doi:10.1029/2006JD007072, 2006.
Takegawa, N., Miyazaki, Y., Kondo, Y., Blake, D. R., Kanaya, Y., Koike, M., Fukuda, M., Komazaki, Y., Miyazaki, Y., Shimono, A., and Takeuchi, T.: Evolution of submicron organic aerosol in polluted air exported from Tokyo, Geophys. Res. Lett., 33, L15814, doi:10.1029/2006GL025815, 2006.
Velasco, E., Lamb, B., Westberg, H., et al.: Distribution, magnitudes, reactivities, ratios and diurnal patterns of volatile organic compounds in the Valley of Mexico during the MCMA 2002 & 2003 field campaigns, Atmos. Chem. Phys., 7, 329–353, 2007, http://www.atmos-chem-phys.net/7/329/2007/.
Volkamer, R., Jimenex, J. L., San Martini, F., Dzepina, K., Zhang, Q., Salcedo, D., Molina, L. T., Worsnop, D. R., and Molina, M. J.: Secondary organic aerosol formation from anthropogenic air pollution: Rapid and higher than expected, Geophys. Res. Lett., 33, L17811, doi:10.1029/2006GL026899, 2006.
Warneke, C., de Gouw, J. A., Stohl, A., et al.: Biomass burning and anthropogenic sources of CO over New England in the summer 2004, J. Geophys. Res., 111, D23S15,

doi:10.1029/2005JD006878, 2006.
Weber, R. J., Sullivan, A. P., Peltier, R. C., Russell, A., Yan, B., Zheng, M., de Gouw, J., Warnke, C., Brock, C., Holloway, J. S., Atlas, E. L., and Edgerton, E.: A study of secondary organic aerosol formation in the anthropogenic-influenced southeastern United States, J. Geophys. Res., 112, D13302, doi:10.1029/2007JD008408, 2007.
Yokelson, R., Urbanski, S., Atlas, E., et al.: Emissions from forest fires near Mexico City, Atmos. Chem. Phys. Discuss., 7, 6687–6718, 2007, http://www.atmos-chem-phys-discuss.net/7/6687/2007/.
Zhang, Q., Worsnop, D. R., Canagaratna, M. R., and Jimenex, J. L.: Hydrocarbon-like and oxygenated organic aerosols in Pittsburgh: Insights into sources and processes of organic aerosols, Atmos. Chem. Phys., 5, 3289–3311, 2005, http://www.atmos-chem-phys.net/5/3289/2005/.
Zhang, Q., Jimenex, J. L., Worsnop, D. R., and Canagaratna, M.: A case study of urban particle acidity and its influence on secondary organic aerosol, Environ. Sci. Technol., 41, 3217–3219, 2007.

Table 1. Flights used in this study.

Flight mdd a or b	Time (LST) in Mexico City Basin	Number of transects L0	L1	L2	L3	L4	L5
306a	11:39–14:04	1	2		1	5	5
307a	12:43–15:03	1	2		1	5	5
315a	10:41–11:49	1	2		1	1	1
318a	14:06–16:39		4	4			
319a	10:38–12:18	1	2	2	1	1	1
320a	10:11–11:44	1	2	2	1	1	1
320b	14:43–16:28		3	3			
322a	10:09–11:50	1	1	2	1	1	1

Table 2. Instruments.

Measurement	Method
CO	VUV fluorescence
NO, NO_2, NO_y	NO chemiluminescence, photolysis of NO_2, reduction to NO by 350°C Mo converter
SO_2	pulsed fluorescence
CH_3CN, toluene, terpenes	PTR-MS
Aerosol composition	C-ToF AMS
Aerosol size distribution	PCASP, SMPS (DMA)
Turbulent energy dissipation rate	gust probe

Table 3. AMS collection efficiency (CE) for urban plume data[1].

Flights	Data Points	CE=slope AMS volume vs. PCASP or DMA volume[1]		
		PCASP<400 nm	PCASP<500 nm	DMA<444 nm
7 Flights[2]	1388	0.54 (0.076)	0.49 (0.085)	0.44 (0.078)
322a	87	0.92	0.87	0.77

[1] Data points are those used in aerosol time dependence calculations with the additional restriction that DMA measurements are available.
[2] Standard deviations in parenthesis show flight to flight variability of CE.

Table 4. Data selection criteria for urban air masses[1].

Criterion to include data	Data that is eliminated
Lon<–98	outside Mexico City plateau
Turbulent energy dissipation rate >0.1 ($cm^2\ s^3$)	free troposphere
CO>100 ppb	possible free tropospheric air
CH_3CN< 0.2 + 0.4 CO/1000	forest fire emissions
15<(CO–100)/NO_y<25 for CO>170 ppb	biomass burning and industrial and utility emissions with CO/NO_y ratios different than observed in high concentration plumes over Mexico City
Org <50 $\mu g\ m^{-3}$	outliers
SO_2<25 ppb	industrial and utility plumes
SO_2<10 ppb near Tula	Tula refinery and power plant plume

[1] In addition, to calculate dilution-corrected aerosol concentration as a function of photochemical age, AMS, CO, NO_x, and NO_y observations must all be available.

Table 5. Factor by which dilution-corrected aerosol concentration increase during atmospheric aging.

Species	Age Growth factor[1]
organics[2]	6.9
Total[2]	5.0
organics[3]	7.0
nitrate[3]	1.8
sulfate[3]	9.5
ammonium[3]	3.6
chloride[3]	3.6

[1] Fractional increase between young and old air masses, defined in Eq. (6).
[2] From regressions vs. CO.
[3] From Eq. (5).

Table 6. Comparison of organic aerosol formation in Mexico City and the U.S.

Age	OA/CO (μg m^{-3} ppm^{-1})[1]		
	Mexico City[2]	NEAQS 2002[2,3]	NEAQS/ITCT 2004[4]
Near source	10	37	6.6
~1day	73	103	70
Change	62	66	63

[1] Aerosol concentration at 20°C, 1 atmosphere.
[2] Age = $-\text{Log}_{10}(\text{NO}_x/\text{NO}_y)$ varies from 0.083 to 0.94.
[3] Data from Kleinman et al. (2007). Aerosol concentration converted from ambient T and P, yielding ~8% increase.
[4] Data from Sullivan et al. (2006) and Weber et al. (2007). Water soluble organic aerosol as measured by a particle into liquid sampler (PILS). Results reported as OC/CO have been converted into OA/CO using 2.2 μg OA/μg OC, as appropriate for OOA.

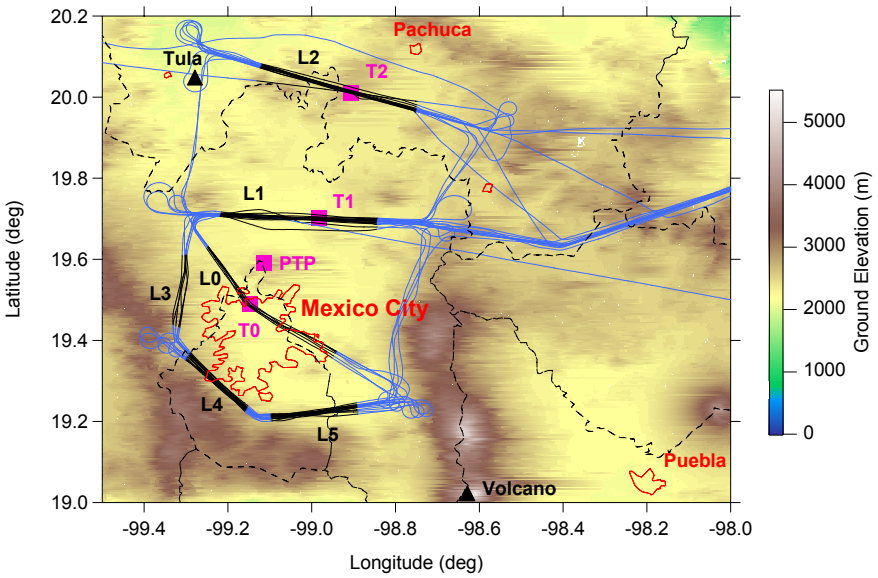

Fig. 1. Part of G-1 sampling area, color coded by surface altitude. Map shows ground track of the 8 flights used in this study. Figure shows surface sites at PTP, T0, T1, and T2. Identified emission sources are Mexico City, Pueblo, Pachuca, the Tula industrial complex, and the Popacatapetl volcano. For presentation and analysis purposes 6 flight legs are defined, L0 to L5. L0, L1, and L2 include overpasses of T0, T1, and T2 surface sites. Data used in this study is restricted to be west of 98° longitude but does not have to lie on legs L0–L5.

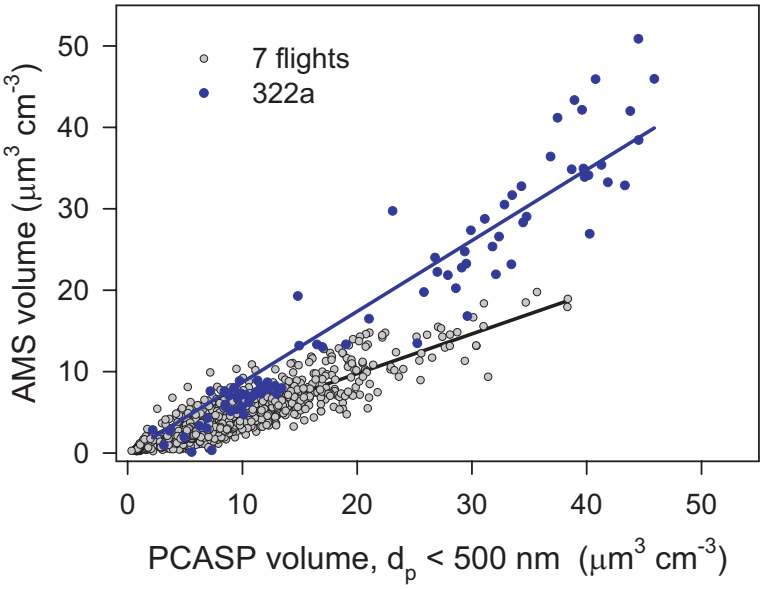

Fig. 2. Comparison of aerosol volume calculated from the AMS with that determined from the PCASP. PCASP volume includes contribution from particles with D_p<100 nm, determined from DMA. Data points are 10 s averages that meet urban plume criteria. Lines are linear least squares fits to data constrained to pass through origin. For the first 7 flights the least squares fit has a slope of 0.49±0.004 and r^2=0.81; for the 322a flight the slope is 0.87± 0.017 and r^2=0.91.

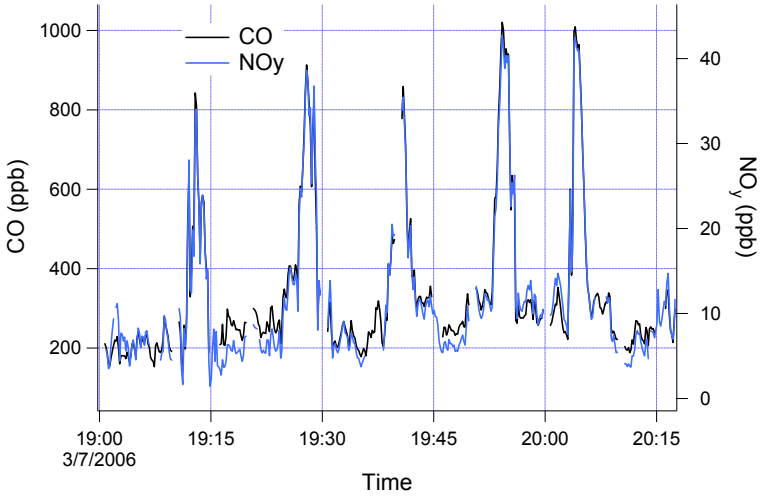

Fig. 3. Time series in UTC for CO and NO_y on flight 307a containing 5 passes through the urban plume encountered on Legs 4 and 5. Proportionality between CO and NO_y causes CO trace to be largely hidden by NO_y trace during plume passages.

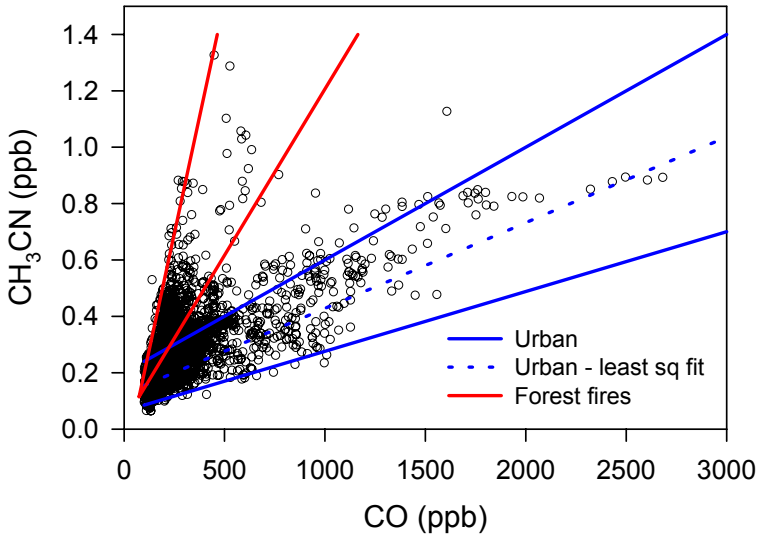

Fig. 4. Scatter plot of CH_3CN vs. CO concentration. Each data point is a 10 s measurement period which satisfies criteria in Table 4 except for the limits on CH_3CN and on $(CO-100)/NO_y$. Red lines encompass the range of CH_3CN – CO relations found in forest fire plumes by de Gouw et al. (2006). Blue lines encompass data points designated as having an urban source of CH_3CN. Bottom blue line is an approximate indication of the lower limit of CH_3CN in urban samples. Data points above the top blue line, given by Eq. (2), are eliminated from subsequent analysis as having a significant forest fire influence.

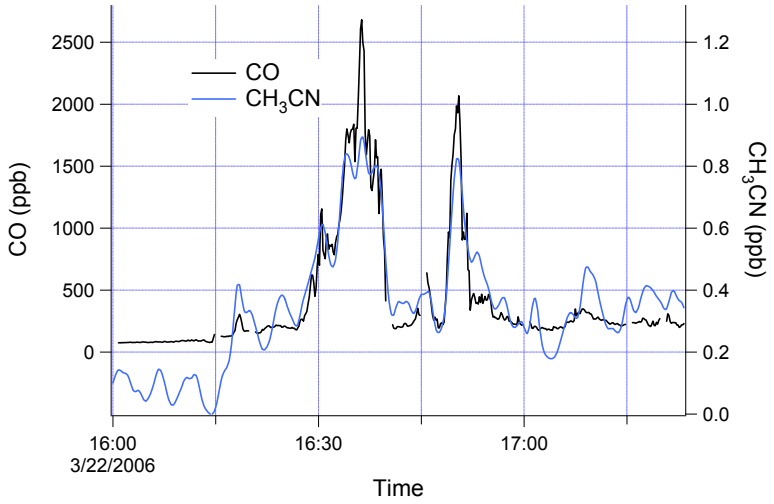

Fig. 5. Time series in UTC for CO and CH_3CN on flight 322a. Urban plume was encountered on L4 (16:35) and then L0 (16:50). Linear least squares regression for urban plume, excluding points with high CH_3CN according to Eq. (2) gave $CO=105 + 21.9\ NO_y$, $r^2=0.97$. The CO and CH_3CN axies are scaled by $CH_3CN=0.2 + 0.4\times10^{-3}$ CO which describes the proportionality between CH_3CN and CO in the urban plume. Points where the CH_3CN (blue) curve are above the CO (black) curve are identified as having a significant biomass burning influence.

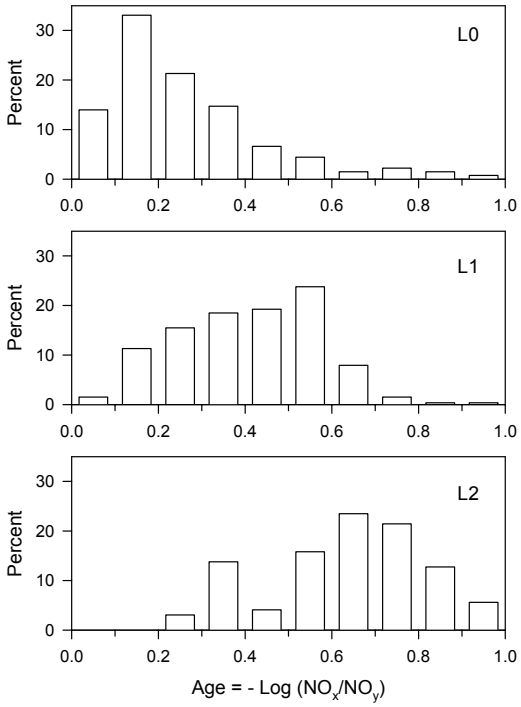

Fig. 6. Frequency distribution of photochemical age for the L0, L1, and L2 flight legs.

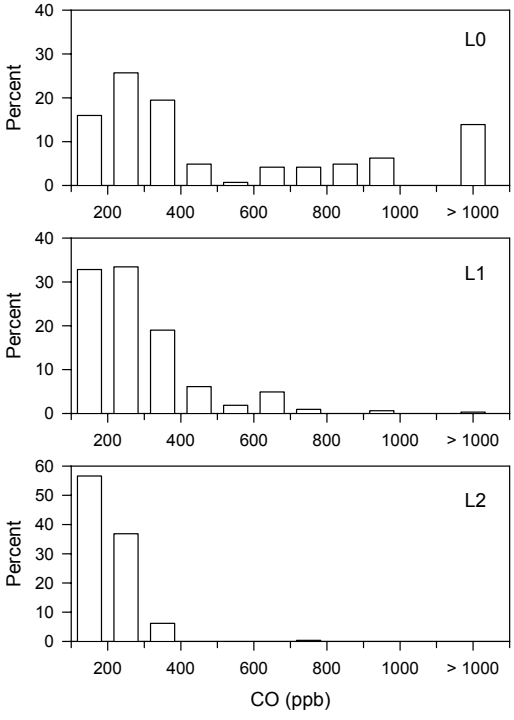

Fig. 7. Frequency distribution of CO for the L0, L1, and L2 flight legs.

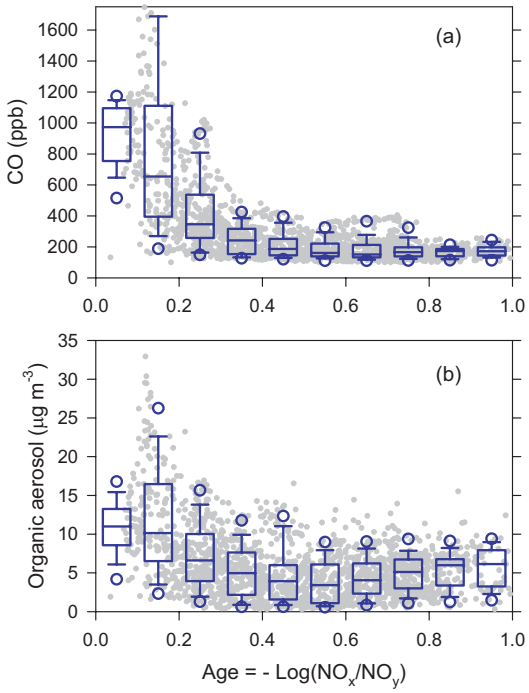

Fig. 8. (a) CO and **(b)** Organic aerosol concentration as a function of photochemical age. Data points are 10 s average values meeting selection criteria in Table 4. Box plots give frequency distribution of data within an age bin. Box shows 75th, 50th(median) and 25th percentile of data. Caps show 90th and 10th percentiles. Circles show 95th and 5th percentiles. For clarity, bins are placed at the midpoint of age intervals. Average age in the first and last bin are 0.083 and 0.94 corresponding to NO_x/NO_y ratios of 83% and 11%, respectively.

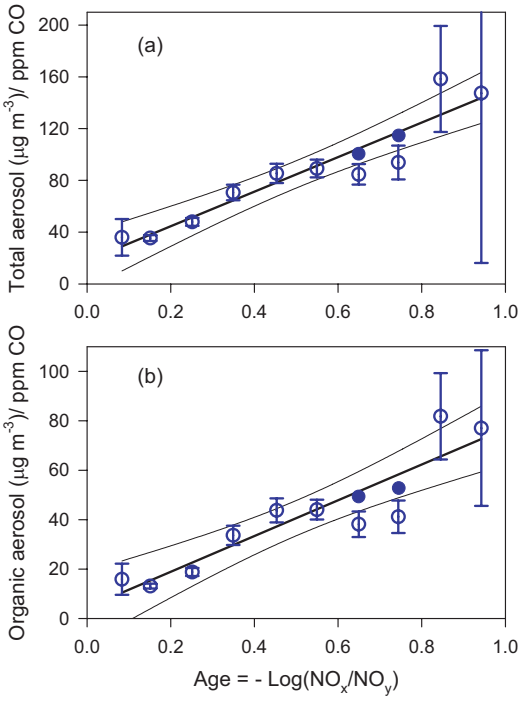

Fig. 9. Slopes from reduced major axis linear regression of **(a)** Total aerosol concentration and **(b)** Organic aerosol concentration vs. CO plotted as a function of photochemical age. Error bars are 2σ, calculated from χ^2 of the regression. (Press et al., 1986). Graphs show linear least squares fit to data points and 95% confidence interval. Solid symbols (not used for least squares fit) are from regressions in which the CO plume on flight 320b was eliminated.

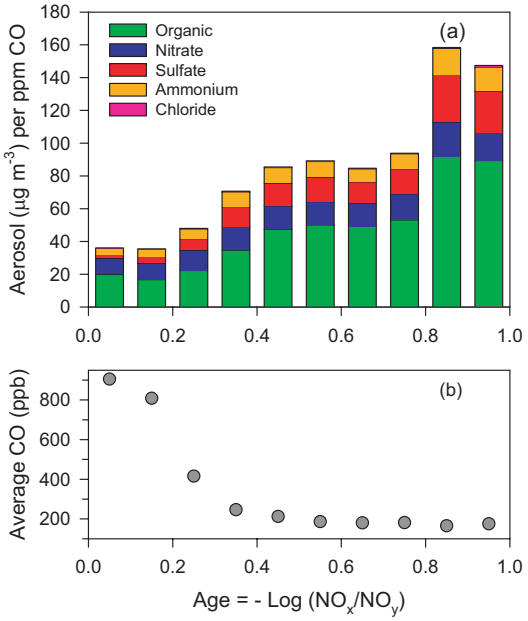

Fig. 10. **(a)** Aerosol concentration per ppm CO and **(b)** CO concentration as a function of photochemical age. For clarity, bars and data points are placed at the nominal centers of the age bins, i.e. at ages 0.05, 0.15, etc. First and second age bins are closer than they appear (see Fig. 9). Speciated aerosol composition in (a) calculated from Eq. (6). Bars representing the sum of the 5 components measured by the AMS have the same magnitude as the data points in Fig. 9a.

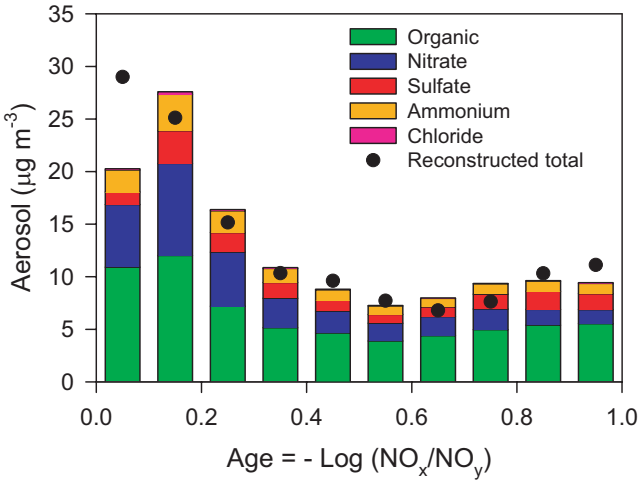

Fig. 11. Speciated ambient aerosol as a function of photochemical age. For clarity bars and data points are placed at nominal center of age bins. The reconstructed total aerosol mass is determined by multiplying aerosol concentration per ppm CO (Fig. 10a) by average CO concentration (Fig. 10b) minus 100 ppb background.

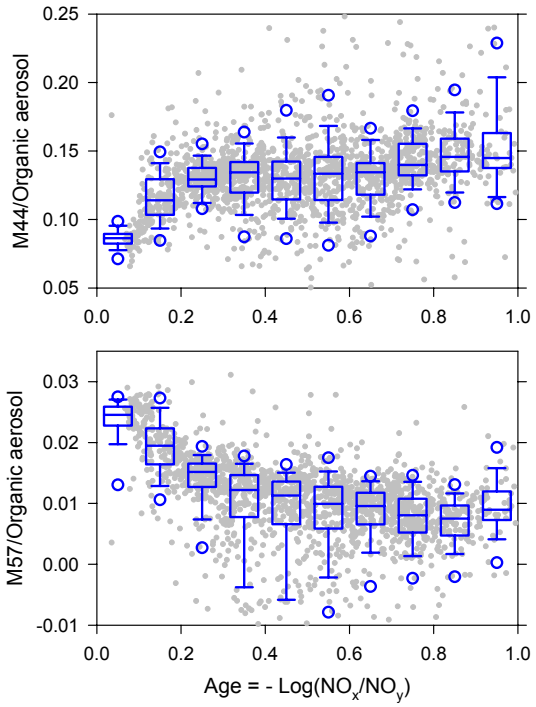

Fig. 12. Fraction of organic aerosol mass that is **(a)** M44 (amu/z=44) and **(b)** M57 (amu/z=57). Box plots have same format as Fig. 8.